ELSEVIER

Chemical Engineering Journal 136 (2008) 50–65

Chemical Engineering Journal

www.elsevier.com/locate/cej

Mass transfer limitations in photocatalytic reactors employing titanium dioxide suspensions I. Concentration profiles in the bulk

María de los Milagros Ballari, Rodolfo Brandi, Orlando Alfano, Alberto Cassano *

INTEC, Universidad Nacional del Litoral and CONICET, Güemes 3450, 3000 Santa Fe, Argentina

Received 12 October 2006; received in revised form 15 March 2007; accepted 19 March 2007

Abstract

The problem of mass transfer limitations in slurry, photocatalytic reactors employing titanium dioxide alone and applied for pollution abatement is studied with simulation experiments resorting to an existing isothermal reactor and making use of a corrected and recalculated intrinsic reaction kinetics previously obtained from a complete reaction mechanism corresponding to the mineralization of dichloroacetic acid. The mathematical description of the reactor is made employing rigorous momentum, radiation and mass transfer models derived from fundamental principles. In the first part of the work the analysis is concentrated in the bulk of the fluid. External and internal catalytic particle (and possible agglomerations) mass transfer limitations are the subject of the subsequent study. The main explored variables were: (i) flow rate, (ii) catalyst loading, (iii) irradiation rates, (iv) virtual changes in one significant kinetic constant of the kinetic model, (v) total suspension volume, and (vi) virtual changes in the reactor illuminated length. Significant concentration gradients that could result in appreciable transport limitations derived from the intrinsic non-uniformity of the radiation field are observed. These concentration gradients are difficult to be avoided, and they can be eliminated only if the reactor is operated under fully developed turbulent flow or very strong mixing conditions. However, it can be concluded that when the photocatalytic reaction is not fast, employing catalyst loadings below 1 g L^{-1}, irradiation rates below 1.0×10^{-7} Einstein cm^{-2} s^{-1} and very good mixing operation, it will be always safe to assume that mass transport limitations in the bulk of the fluid are inexistent.
© 2007 Elsevier B.V. All rights reserved.

Keywords: Photocatalysis; Slurry reactors; Global mass transfer limitations; Unsupported titanium dioxide

1. Introduction

Contaminated waters even with low concentrations of pollutants have been a problem of increasing concern in communities living in the vicinity of raw water sources for domestic use located close to wastewater drainages. Several new purification processes grouped under the common denomination of Advanced Oxidation Technologies may provide potential solutions to these justified worries.

These new technologies have two distinctive advantages compared with more traditional ones: (1) they make use of destructive reactions that in the vast majority of the cases transform pollutants into innocuous products [1–3] and (2) these reactions have very low selectivity, thus permitting the treatment of a wide range of contaminants such as: herbicides [4], pesticides [5,6], phenol and its derivatives [7–9], halocarbonated compounds [10,11], alcohols [12,13], organic acids [14–16], and dyes [17,18]. Among them, photocatalysis is one of the most extensively investigated. For various reasons repetitively reported, titanium dioxide has been the preferred choice [19].

One important aspect concerning the use of solid catalytic semiconductors is the existence of two alternatives associated with the decision to use suspensions of small catalytic particles, which normally have been reported to yield the best activity [20–25] but have the drawback of additional downstream separation costs or, alternately, the adoption of different forms of immobilized titanium dioxide in various reactor configurations [24,26–31]. In some of the latter it is well-known that mass transfer limitations have been frequently reported [16–18,23,24,26–28,32–37]. In the case of slurry reactors, employing pure titanium dioxide, the problem has not been thoroughly studied with a few exceptions such, as for example, valuable contributions by (i) Bideau et al. [38] somewhat limited due to the use of oversimplified reaction kinetics and

* Corresponding author. Fax: +54 342 4511087.
E-mail address: acassano@ceride.gov.ar (A. Cassano).

1385-8947/$ – see front matter © 2007 Elsevier B.V. All rights reserved.
doi:10.1016/j.cej.2007.03.028

Nomenclature

a_v	solid–liquid interfacial area per unit reactor volume ($cm^2\ cm^{-3}$)
A	area (cm^2)
C_A	molar concentration of component A ($mol\ cm^{-3}$)
C_{mc}	mass concentration of catalyst ($g\ cm^{-3}$)
C_{O_2}	molar concentration of oxygen ($mol\ cm^{-3}$)
$\mathcal{D}_{A,mix}$	pseudo-binary diffusion coefficient ($cm^2\ s^{-1}$)
$\mathcal{D}_{A,turb}$	eddy turbulent diffusion coefficient ($cm^2\ s^{-1}$)
e^a	local volumetric rate of photon absorption (Einstein $s^{-1}\ cm^{-3}$)
e^a_S	local superficial rate of photon absorption (Einstein $s^{-1}\ cm^{-2}$)
f	friction coefficient
g	parameter in the phase function for scattering
G	incident radiation (Einstein $s^{-1}\ cm^{-2}$)
H	depth (cm)
I	specific radiation intensity (Einstein $s^{-1}\ cm^{-2}\ sr^{-1}$)
k	kinetic constant, units depend on the reaction step
K	equilibrium constant ($cm^3\ mol^{-1}$)
L	length (cm)
p	phase function
Q	volumetric flow rate ($cm^3\ s^{-1}$)
R_{Het}	heterogeneous reaction rate ($mol\ s^{-1}\ cm^2$)
Re	Reynolds number
s	directional spatial coordinate (cm)
S_g	specific catalyst surface area ($cm^2\ g^{-1}$)
t	time (s)
v	velocity ($cm\ s^{-1}$)
V	volume (cm^3)
W	width (cm)
y	Cartesian coordinate (cm)
z	Cartesian coordinate (cm)

Greek letters

Φ	quantum yield ($mol\ Einstein^{-1}$)
Ω	solid angle (sr)
$\underline{\Omega}$	unit vector in the direction of radiation propagation
α_1	kinetic parameter ($cm^4\ mol^{-1}\ s^{-1}$)
α_2	kinetic parameter ($cm^4\ s^{-1}\ Einstein^{-1}$)
β	volumetric extinction coefficient (cm^{-1})
δ_y	parameter in the variable change in the y-direction for the numerical solution of the mass balance equation
δ_z	parameter in the variable change in the z-direction for the numerical solution of the mass balance equation
φ	z coordinate in the transformed space (cm)
κ	volumetric absorption coefficient (cm^{-1})
λ	wavelength (nm)
μ	$\cos\theta$
μ_0	cosine of the angle between an incoming and a scattered ray
ν	kinematic viscosity ($cm^2\ s^{-1}$)
θ	spherical coordinate (rad)
σ	volumetric scattering coefficient (cm^{-1})
τ	mean residence time (s)
ξ	y coordinate in the transformed space (cm)

Subscripts

ads	denotes adsorption
A	component A
c	catalyst
ex	exit condition
in	inlet condition
max	maximum value
mix	mixture
R	reactor
S	relative to superficial variable
T	total
Tk	tank
turb	turbulent
W	relative to the wall of the reactor
z	relative to z-axis
Ω	relative to the direction of radiation propagation
λ	relative to wavelength

Superscripts

H_R	surface at $y = H_R$
0	initial value; also surface at $y = 0$
*	specific properties

Special symbols

$\langle\ \rangle$	average value over a defined space
under bar	a vector value
over bar	average value over wavelengths

radiation transport equations, (ii) Chen and Ray [8] that did not find significant diffusive limitations in suspended solid reactors, (iii) a more detailed experimental study by Mehrotra et al. [39] that have found that at high catalyst loadings there are both internal diffusive and light penetration restrictions providing qualitative explanations for the obtained results and (iv) Martín et al. [40] that, proposing a rather simple kinetics for a reaction performed in an annular reactor and employing a rigorous theoretical model, studied the effects produced by changes in the optical thickness of the reaction space (resulting from variation in the catalyst loadings) on the local volumetric rate of photon absorption and the reactor conversion. Computational results were presented for both the radial and axial directions, showing the consequent lost of efficiency when the said optical thickness exceeded the calculated optimal values. On the other hand, the literature concerning experimental observations reporting very different limiting values of the catalyst concentrations beyond which the reaction rate reaches a plateau or appreciably decreases is more abundant [10,12,41–49]. Furthermore, Bickley et al. [50], considered farther this problem, reporting the results of several studies considering changes in the

reaction rate with variations in the catalyst concentration, indicating that in some cases the optimal concentration was reached before the point where the reactor became opaque and, in others, larger conversions were observed after reaching this optical condition [40,41,47–49]. They mentioned that most of the explanations for these phenomena were given without quantification or convincing arguments and that this problem must be solved to assist any effort directed towards photocatalytic reactor design.

This work is an attempt to quantify these effects, in many cases produced by mass transport limitations, and extend the results shown by Martín et al. [40] including additional variables and operating conditions as well as a more realistic kinetics. This phenomenon is important in both, kinetics studies to obtain intrinsic parameters free from mass transfer limitations and reactor design to operate the equipment under the most efficient conditions. Very often, in laboratory studies with suspended catalysts, mixing is achieved with a gentle magnetic stirring in reactors of regular size, which may give rise to doubts concerning the generalized use of the perfect mixing assumption in the interpretation of the results.

There are several problems to examine but the interrelationship among them must be investigated to explain three phenomena: (i) often, the reaction rate increases beyond the catalyst concentration that makes the reaction space opaque transforming, from the radiation absorption point of view and, analyzing the phenomenon independently, part of the reactor volume is theoretically useless [51], (ii) under some experimental conditions the observed reaction rates reach a maximum and afterwards decrease with increasing the catalyst concentration [39,41,47–49], and (iii) when the irradiation intensities arriving to the reactor reach high values, the reaction rate becomes unaffected by further increases in the radiation energy input [39,52].

The essential point is to recognize that in photocatalytic slurry reactors there are different interrelated phenomena that analyzed separately may lead to erroneous conclusions and, at the same time, their effects are difficult to investigate when they are considered simultaneously: (i) examining radiation transport, increasing the catalyst concentration, there is a limit in the characteristic distance of radiation propagation (that can be expressed in terms of an optical thickness) beyond which, in practical terms, all the incoming radiation has been absorbed and, in the absence of very strong mixing, beyond this distance it is true that no further catalyst activation is possible; (ii) however, being a catalytic reaction the number of active sites increases with catalyst concentration disguising the effects related to the existence of very large optical thickness; (iii) increasing the catalyst concentration (or, in other terms, the available surface area or active sites, or the optical thickness) its effect in the reaction rate may turn possible that diffusive limitations of reactants and/or products come into scene with several possible mechanisms (severe concentration gradients in the bulk, interfacial external diffusion and even internal diffusion due to catalyst porosity and especially agglomeration); (iv) increasing the incident radiation on the catalytic surface may have similar effects on the reaction rate, giving rise to analogous diffusive limitations; (v) in porous catalytic particles (very often due to catalyst agglomeration) the light penetration may not be complete and part of the catalyst nominal surface area may be useless; this last phenomenon may be coupled with internal diffusive limitations of reactants and/or products. The existence of these interrelated phenomena will be emphasized throughout this work, particularly in the graphical representation of the obtained results. Catalytic external surface limitations and catalytic particle (or agglomerates) internal transport limitations of both mass and radiation transport will be the subject of a separate contribution.

Resorting to a previous work [53], but introducing some changes in the kinetic model, due to the existence of an unjustified assumption, and recalculating all the kinetic parameters from the original data [54], a realistic, mechanistically derived, intrinsic reaction kinetics was used. Afterwards, resorting to simulation experiments and making use of rigorous mass and radiation transport models, some of the above described phenomena will be analyzed in this contribution. The main problems are: (i) the limiting operating conditions under which diffusive limitation in the bulk of the reactor space produce important distortions in the interpretation of experimental results and (ii) the definition of conditions under which these effects are safely negligible. This first part will be concerned exclusively with global concentration gradients.

The strategy for the analysis is to consider first the solution of the differential mass balance and radiation transport equations for a specially designed photoreactor with a sort of global approach looking at the field of concentration in the bulk, with and without the assumption of complete mixing, and observe under which conditions radiation and concentration profiles can arise. Pivoting around the operating conditions of the modified work of Zalazar et al. [53] and thus obtaining a validated and intrinsic kinetic expression for dichloroacetic acid degradation, the effects produced by changes in the following variables will be inspected in the simulation studies: (i) the catalyst concentration, (ii) the flow rate, (iii) the irradiation rates, (iv) the catalytic activity (resorting to virtual changes in the appropriate kinetic constant), (v) the total suspension volume, and (vi) the effects resulting from a significant change in the reactor length (to avoid disguising results as a consequence of an unwanted differential operation of the reactor).

2. Description of the adopted experimental set up

This simulation work was not done in abstract. All the parameters correspond to a reactor presently under operation. The apparatus is assembled with the following components (Fig. 1 and Table 1): (i) one long parallelepiped (100 cm × 8 cm × 1 cm) that includes, in a small part of its length (at its top), one flat plate photoreactor resulting from the existence of one borosilicate glass window (15 cm × 8 cm) on each side of the parallelepiped; (ii) a recirculating centrifugal pump; (iii) a rotameter; (iv) a well-stirred, 5000 cm^3 tank, isolated from the laboratory light (employing two different liquid volumes: 500 and 3000 cm^3); (v) an oxygen bubbling system, operating continuously in the tank to maintain constant the gas concentration in the reactor feed; (vi) a heat exchanger for temperature control connected

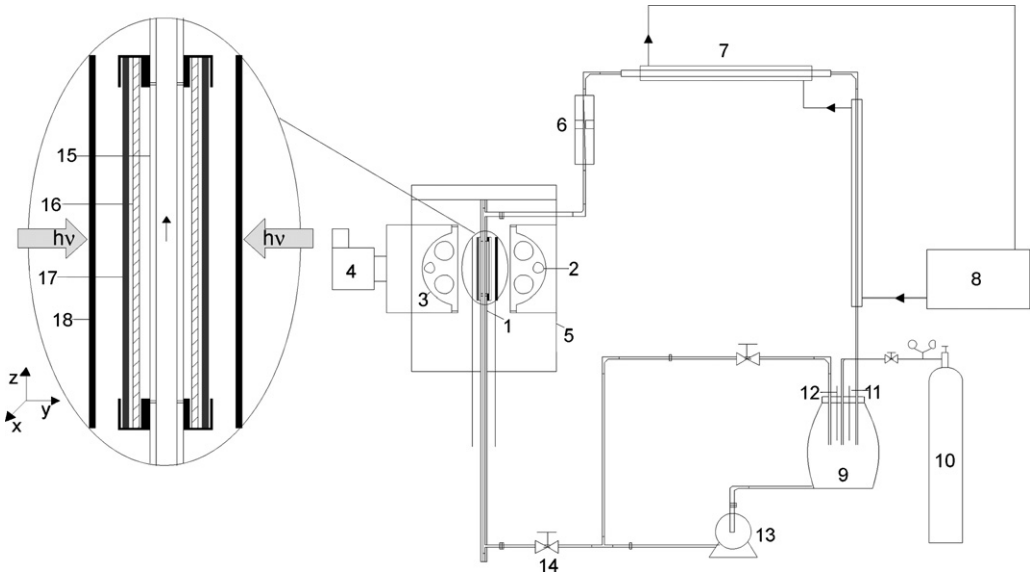

Fig. 1. Reactor description. Keys: 1, reactor; 2, UV lamp; 3, parabolic reflector; 4, blower; 5, box; 6, flowmeter; 7, heat exchanger; 8, thermostatic bath; 9, tank; 10, oxygen; 11, sampling; 12, thermometer; 13, pump; 14, valve; 15, borosilicate glass window; 16, borosilicate ground glass; 17, neutral filter; 18, shutter.

to a thermostatic bath; (vii) two lamps (one on each side of the windows) located horizontally at the focal axis of their respective custom made parabolic reflectors. The radiation sources are medium pressure, Mercury lamps with a nominal input power of 1000 W each (chosen to have the possibility of investigating a wide range of irradiation rates) and polychromatic emission between 260 and 580 nm with a well-known quantitative relative wavelength distribution of the output energy; (viii) between each lamp system and the reactor window there are a flat borosilicate ground glass to produce diffuse emission toward the reaction space and neutral density filters of different transmissions to change the intensity of the incident radiation on the reactor windows; (ix) the lamps and reflectors operating temperatures are controlled. With this arrangement, considering the radiation absorption characteristics of titanium dioxide, the reflecting properties of the aluminum mirrors and the transmission characteristics of the borosilicate glass, the useful wavelength range for operation is between 275 and 390 nm. When the wavelength distribution of the lamp output is known, Zalazar et al. [55] have developed a method to calculate the incident radiation on the reactor window in the specific useful wavelength working range, from actinometric measurements in the whole range of emission by the lamp.

Table 1
Adopted reactor main characteristics

Reactor: stainless steel	
Length	100 cm
Width	8 cm
Thickness	1 cm
Total volume	800 cm^3
Reactor windows: borosilicate glass	
Length	15 cm
Entrance length	75 cm
Width	8 cm
Thickness	1 cm
Photoreactor volume	120 cm^3
Nominal recirculating volume	3000 cm^3 and 500 cm^3
Recirculating pump: stainless steel	
Operating power	0.5 hp
Lamps: Philips HPA 1000 × 2	
Input power	1000 W
Length	8.5 cm
Emission wavelength	260–580 nm
Reflectors: aluminum mirrors	
Alzac® treatment	Parabolic
Filters: neutral density	
Filters attenuation	7, 20 and 45%
Tank: glass	
Volume	5000 cm^3
Catalyst: TiO_2	
Aldrich	99% Anatase

3. Theoretical models

Either for a laboratory reactor or a large scale apparatus, the problem always starts by writing the mass balance. Depending on the operating conditions, the required information from the momentum balance may be very simple (even unnecessary) or more complex, but the velocity field must be well-defined. The mass balance in a reacting system will ask for a reaction rate either in the differential equation or in the boundary conditions for heterogeneous systems. This reaction may be an empirical, phenomenological proposition or, much better, a mechanistically derived expression. The distinctive characteristic of photochemical reactions is that the above mentioned reaction rate always involves at least one activation step produced by absorption of radiant energy. Consequently a radiation balance is needed. Under isothermal conditions, the thermal energy balance may not be necessary on account that the energy associated with those photons having the ability to activate reactions has very low thermal effects and the uncoupling of the

radiation balance from the thermal energy balance is an accepted simplification in the majority of the cases. We will formulate our approach following the above described steps. For the reaction kinetics, the photocatalytic mineralization of the dichloroacetic acid will be used. It has already been shown [53] that in the employed useful wavelength range there is no homogeneous reaction.

For the momentum balance, under well developed velocity profile in laminar regime (recall the described entrance length in Table 1):

$$v_{z,S}(y) = v_{max}\left[1 - \left(\frac{2y}{H_R} - 1\right)^2\right] \quad (1)$$

With:

$$v_{max} = \frac{3Q}{2H_R W_R} \quad (2)$$

Whereas for turbulent flow the von Karman velocity profile near the wall [56,57] and a widely accepted empiric correlation for the turbulent core [58] have been adopted.

For the viscous sublayer:

$$v_z^* = y^*; \quad y^* < 5 \quad (3)$$

For the buffer zone:

$$v_z^* = 5\ln y^* - 3.05, \quad 5 < y^* < 30 \quad (4)$$

For the turbulent core:

$$v_z^* = 2.5\ln\left[y^*\frac{3(1-(y/H_R))}{1+2(1-(2y/H_R))^2}\right] + 5.5, \quad y^* > 30 \quad (5)$$

With:

$$v_z^* = \frac{v_{z,S}}{\langle v\rangle^*}; \qquad y^* = \frac{y\langle v\rangle^*}{\nu} \quad \text{and} \quad \langle v\rangle^* = \sqrt{\frac{f}{2}}\langle v_{z,S}\rangle \quad (6)$$

where y^* goes from the wall to the center of the flat plate and f is the friction coefficient, which for turbulent flow can be calculated from [58,59]:

$$f = \frac{0.0791}{Re^{1/4}}; \quad 2.1\times 10^3 < Re < 10^5 \quad (7)$$

The mass balance of component "A" for a heterogeneous reaction considered as a boundary condition in a flow reactor, with the pseudo-homogeneous assumption, applying a two-dimensional model and considering constant temperature, density and viscosity results [57,59,60]:

$$\frac{\partial C_{A,R}(y,z,t)}{\partial t} + v_{z,S}(y)\frac{\partial C_{A,R}(y,z,t)}{\partial z} - \frac{\partial}{\partial y}\left\{[\mathcal{D}_{A,mix} + \mathcal{D}_{A,turb}(y)]\frac{\partial C_{A,R}(y,z,t)}{\partial y}\right\} = a_V R_{Het,A,R}(y,z,t) \quad (8)$$

In those cases operating under laminar flow regime, the pseudo-binary diffusivity ($D_{A,mix}$) is used considering the usually very dilute concentration of the contaminant in the mixture for those cases in which photocatalysis could be applicable. On the other hand, the eddy turbulent diffusion coefficient ($D_{A,turb}$) is used in the turbulent regime cases, and was calculated using an empirical correlation [58,61,62]. In addition, considering the employed catalyst concentrations, the solid hold-up is practically negligible.

For the tank, and again for a heterogeneous system, with a similar reasoning, we can get:

$$\frac{dC_{A,Tk,ex}(t)}{dt} = \frac{Q}{V_{Tk}}[C_{A,Tk,in}(t) - C_{A,Tk,ex}(t)] \quad (9)$$

The initial and boundary conditions for the system are:

$$C_{A,R}(y,z,t=0) = C_{A,R}^0 \quad (10)$$

$$\frac{\partial C_{A,R}(y=0,z,t)}{\partial y} = 0 \quad (11)$$

$$\frac{\partial C_{A,R}(y=H_R,z,t)}{\partial y} = 0 \quad (12)$$

The connecting conditions between reactor and tank are:

$$C_{A,R,in}(y,z=0,t) = C_{A,Tk,ex}(t) \quad (13)$$

$$C_{A,Tk,in}(t) = \langle C_{A,R,ex}(y,z=L_R,t)\rangle_{A_R} = \frac{\int_{y=0}^{y=H_R} C_{A,R}(y,z=L_R,t)v_{z,S}(y)\,dy}{\int_{y=0}^{y=H_R} v_{z,S}(y)\,dy} \quad (14)$$

According to Appendix A and using the original data of Zalazar [54] the following reaction kinetic model corresponding to the reaction described in Table 2, will be employed:

$$a_V R_{Het,A}(y,z,t) = S_g C_{mc}\alpha_1 C_{A,R}(y,z,t)C_{O_2} \times\left\{1 - \sqrt{1 + 2\frac{\alpha_2}{\alpha_1^2 S_g C_{mc} C_{A,R}(y,z,t)C_{O_2}}\int_{\lambda=275}^{\lambda=390} e_\lambda^a[(y),C_{mc}]\,d\lambda}\right\} \quad (15)$$

With the following parameters:

$$\alpha_1 = 2.35 \pm 0.42\ \text{cm}^4\ \text{mol}^{-1}\ \text{s}^{-1} \quad \text{and}$$
$$\alpha_2 = 1.25 \pm 0.41\ \text{cm}^4\ \text{s}^{-1}\ \text{Einstein}^{-1} \quad (16)$$

Table 2
Reaction mechanism

Reaction steps	No.	Constants
$TiO_2 + h\nu \rightarrow h^+ + e^-$	0	Φ_λ
$Site + CHCl_2COO^- \leftrightarrow CHCl_2COO_{ads}{}^-$	1	K_1
$CHCl_2COO_{ads}{}^- + h^+ \rightarrow CHCl_2COO^\bullet$	2	k_2
$CHCl_2COO^\bullet \rightarrow HCl_2C^\bullet + CO_2$	3	k_3
$Site + O_2 \leftrightarrow O_{2ads}$	4	K_4
$O_{2ads} + HCl_2C^\bullet \rightarrow CHCl_2OO^\bullet$	5	k_5
$2CHCl_2OO^\bullet \rightarrow 2COCl_2 + H_2O_2$	6	k_6
$COCl_2 + H_2O \rightarrow CO_2 + 2HCl$	7	k_7
$h^+ + e^- \rightarrow Heat$	8	k_8
$O_{2ads} + e^- \rightarrow O_2{}^{\bullet -}$	9	k_9
$O_2{}^{\bullet -} + H^+ \rightarrow HO_2{}^\bullet$	10	k_{10}
$HO_2{}^\bullet + e^- \rightarrow HO_2{}^-$	11	k_{11}
$HO_2{}^- + H^+ \rightarrow H_2O_2$	12	k_{12}

Reaction scheme taken from Zalazar et al. [53].

In Eq. (16) α_1 and α_2 are the lumped kinetic parameters and both include the specific constant for the recombination rate of electrons and holes. This specific constant will be used to introduce virtual changes in the reaction rate in order to make more comprehensive the analysis performed in this work for reactions that could be faster than the DCA degradation.

Finally, the existence of the term $e^{a}_{\lambda}[(y), C_{mc}]$ makes necessary the solution of the radiative transfer equation (RTE) in a participating media, with absorption and scattering (no emission is considered because AOT reactions are normally carried out at ambient temperature) [63,64]:

$$\frac{dI_{\lambda,\underline{\Omega}}(s,t)}{ds} + \underbrace{\kappa_\lambda(s,t)I_{\lambda,\underline{\Omega}}(s,t)}_{\text{ABSORPTION}} + \underbrace{\sigma_\lambda(s,t)I_{\lambda,\underline{\Omega}}(s,t)}_{\text{OUT-SCATTERING}} = \underbrace{\frac{\sigma_\lambda(s,t)}{4\pi}\int_{\Omega'=4\pi} p(\Omega'\rightarrow\Omega)I_{\lambda,\underline{\Omega}'}(s,t)\,d\Omega'}_{\text{IN-SCATTERING}} \quad (17)$$

For the case of a one-dimensional slab geometry (Fig. 2) with azimuthal symmetry (resulting from the diffuse radiation as a consequence of the employed ground glass device) the RTE becomes [65]:

$$\mu\frac{dI_\lambda(y,\mu)}{dy} + (\kappa_\lambda+\sigma_\lambda)I_\lambda(y,\mu) = \frac{\sigma_\lambda}{2}\int_{\mu'=-1}^{\mu'=1} I_\lambda(y,\mu')p(\mu,\mu')\,d\mu' \quad (18)$$

Note that $\kappa_\lambda+\sigma_\lambda=\beta_\lambda$, the extinction coefficient and $\mu=\cos\theta$.

The diffuse and isotropic inlet boundary conditions are:

$$I_\lambda(y=0,\mu) = I^0_\lambda, \quad \text{for } \mu>0 \quad (19)$$

$$I_\lambda(y=H_R,\mu) = I^{H_R}_\lambda, \quad \text{for } \mu<0 \quad (20)$$

According to [66] we will use the Henyey and Greenstein phase function [67,68]:

$$p_{HG,\lambda}(\mu_0) = \frac{1-g^2_\lambda}{(1+g^2_\lambda-2g_\lambda\mu_0)^{3/2}} \quad (21)$$

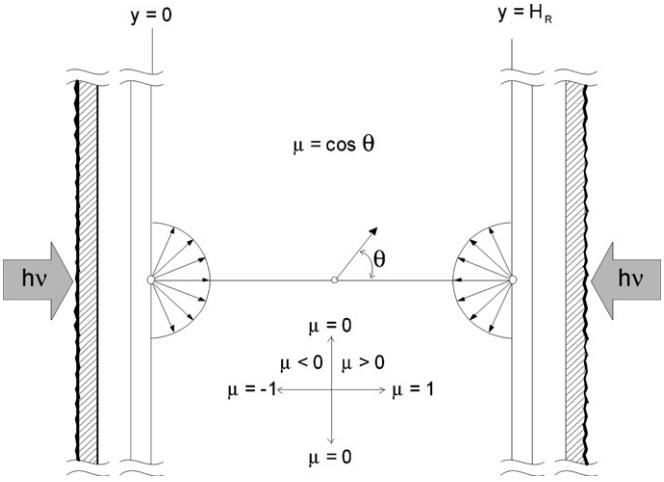

Fig. 2. Schematic representation of the radiation field inside the reactor.

with μ_0 being the cosine of the angle between the direction of propagation of the incoming scattered ray and that for which the RTE is written.

From the values of Specific Intensities, the local volumetric rate of photon absorption (LVRPA) results:

$$e^{a}_{\lambda}[(y), C_{mc}] = \kappa_\lambda\left\{2\pi\int_{\mu=-1}^{1} I_\lambda[(y,\mu), C_{mc}]\,d\mu\right\} \quad (22)$$

3.1. The pseudo-stationary state simplification in the reactor mass balance

This simplification, that should be more valid when the residence time in the reactor is very short and/or when the reaction rate is slow, consists in considering that, during each residence time in the flat plate photoreactor, the inlet concentration to the continuous reactor coinciding with the exit concentration from the tank, remains constant, i.e., during each residence time in the reactor, the concentration in the tank remains constant. Eq. (8) is changed to:

$$v_{z,S}(y)\frac{\partial C_{A,R}[(y,z),t]}{\partial z} - \frac{\partial}{\partial y}\left\{[\mathcal{D}_{A,mix}+\mathcal{D}_{A,turb}(y)]\frac{\partial C_{A,R}\left[(y,z),t\right]}{\partial y}\right\} = a_V R_{Het,A,R}[(y,z),t] \quad (23)$$

For each j cycle, from t_j to $t_j+\tau_R$:

$$C_{A,R}[(y,z=0),t_j] = C_{A,Tk,ex}(t_j) \quad (24)$$

and:

$$C_{A,Tk,in}(t_j+\tau_R) = \langle C_{A,R,ex}(y,z=L_R,t_j+\tau_R)\rangle_{A_R} = \frac{\int_{y=0}^{y=H_R} C_{A,R}(y,z=L_R,t_j+\tau_R)v_{z,S}(y)\,dy}{\int_{y=0}^{y=H_R} v_{z,S}(y)\,dy} \quad (25)$$

3.2. The perfect mixing system

A limiting operation of the system could be achieved if the reactor operates with differential conversion, and/or the reactor volume is very much smaller than the total reaction volume ($V_R/V_T \ll 1$), and the tank and the reactor are well stirred. Then, as shown in [69], considering once more the heterogeneous reaction as a boundary condition:

$$\frac{dC_{A,Tk}(t)}{dt} = \frac{V_R}{V_T}a_V\langle R_{Het,A}(y,t)\rangle_{A_{S,R}} \quad (26)$$

With:

$$C_A(t=0) = C^0_A \quad (27)$$

3.3. Numerical solution and model parameters

Solution of the parabolic differential equations (Eqs. (8) and (23)) for the reactor was numerically obtained using a Crank–Nicholson Finite Difference Method. An important problem to solve was produced by the extremely steep gradients in the LVRPA profiles in regions closed to the windows of radiation entrance. Not with the same degree of difficulty, a similar approach was also needed in the axial direction. The problem was solved with a change of variables [70] according to:

$$\varphi(z) = L_R \left[\frac{1 - \tanh^{-1}\left[(1-z)/L_R\sqrt{1-\delta_z}\right]}{\tanh^{-1}(1-\delta_z)} \right] \quad (28)$$

$$\xi(y) = H_R \left[\frac{\tanh^{-1}\left[(1-(2y/H_R))\sqrt{1-\delta_y}\right]}{\tanh^{-1}(1-\delta_y)} \right] \quad (29)$$

The mass balance for the tank was solved with a Runge–Kutta algorithm. It is interesting to note that stable solutions were obtained when very short time intervals where chosen for the numerical solution of the equations with transient components (Eqs. (8) and (9)).

For both Eq. (8) and Eq. (23) we need a value of the diffusivity of very dilute concentrations of DCA in water. The following result was obtained with different predictive models as described in Table 3. A value of $D_{A,mix} = 8.7 \times 10^{-6}\,cm^2\,s^{-1}$ was adopted for all calculations. For the case of turbulent flow, the following correlation was used to calculate the eddy turbulent diffusion coefficient [62]:

$$\frac{\mathcal{D}_{A,turb}}{\nu_{turb}} = 1.2 - 1.3 \quad (30)$$

Where the eddy turbulent viscosity (ν_{turb}) was estimated with an empiric equation consistent with Eq. (5) for the turbulent core of the photoreactor [58,61,62]:

$$\frac{\nu_{turb}}{\nu} = \frac{0.4y^*}{3}\left[1 + \frac{y}{H_R}\right]\left[1 + 2\left(1 - \frac{2y}{H_R}\right)^2\right] \quad (31)$$

The maximum obtained value of $\mathcal{D}_{A,turb}$ was $0.35\,cm^2\,s^{-1}$ at $y = 0.25H_R$ and $y = 0.75H_R$ for a flow rate equal to $1000\,cm^3\,s^{-1}$. On the walls $\mathcal{D}_{A,turb} = 0$.

The solution of the RTE using the Discrete Ordinate Method [74], employing polychromatic light must resort to three discretizations: a spatial, conventional discretization, a directional or angular discretization (to account for the angular variations of the radiation propagation resulting from multiple scattering), and a spectral discretization (in order to describe the effects of the employed polychromatic radiation). For more details, the reader can find ampler information in [65].

Table 3
Estimation of the pseudo-binary liquid diffusion coefficient at infinite dilution of DCA

Equation	$\mathcal{D}_{A,mix}$ ($cm^2\,s^{-1}$) × 10^6	Reference
Wilke–Chang	8.78	[71]
Scheibel	8.68	[72]
Wayduk Laudie	8.74	[72]
Tyn–Calus	9.01	[71]
Hayduk–Minhas	8.75	[71]
Siddiqi–Lucas	8.04	[73]

Table 4
Spectral distribution of the catalyst optical properties and the relative emission of the lamp

Wavelength (nm)	β^*_λ ($cm^2\,g^{-1}$)	κ^*_λ ($cm^2\,g^{-1}$)	g_λ ($-1 \le g_\lambda \le 1$)	Energy distribution (E_λ/E_T)
275	35,630	8531	0.823	0.0104
305	35,630	8531	0.823	0.0431
310	35,877	8797	0.823	0.0526
324	36,473	8922	0.816	0.033
359	39,750	4750	0.57	0.085
370	40,500	2200	0.47	0.139
385	41,433	379	0.41	0.104

Data taken from Zalazar et al. and Satuf et al. [55,66]. Adopted catalyst: Aldrich (>99.9% Anatase, Cat. 23203-3, lot 10908DZ). Irradiation from each side of the reactor has the following values: $I_{W,\Sigma\lambda,100\%} = 2.93 \times 10^{-7}$ Einstein $cm^{-2}\,s^{-1}\,sr^{-1}$, $G_{W,\Sigma\lambda,100\%} = 1.84 \times 10^{-6}$ Einstein $cm^{-2}\,s^{-1}$.

The selected catalyst for this study was Aldrich (>99.9% Anatase). The values of the dimensionless asymmetry factor g_λ and other optical properties of the adopted catalyst are given in Table 4. The adopted value of the total incident radiation ($275 \le \lambda \le 390$ nm) from each side of the reactor and without filters, measured with potassium ferrioxalate actinometry was [53,55]: $G_W = 1.84 \times 10^{-6}$ Einstein $cm^{-2}\,s^{-1}$.

3.4. Comparison of the transient reactor operation and the pseudo-steady state reactor model approximation

Before getting into the analysis of the effects of the different variables and mass transfer resistances it is convenient to know to what extent the pseudo-steady state model for the proposed reaction in a photocatalytic slurry reactor with recycle, can be used in substitution of the more exact description that considers the transient operation of the same reactor. This amounts to know how significant are the differences in the predictions resulting from the solution provided by Eqs. (1)–(15) and (18)–(22) when Eqs. (8), (13) and (14) are substituted by Eqs. (23)–(25). In both cases, for comparison purposes, the outcome from the model considering perfect mixing everywhere (Eqs. (26) and (27)), without any sort of mass transfer limitations will also be reported.

The first important result to be remarked is that the tank fluid volume exercises a decisive damping effect on the differences between the three models under comparison. Concentrations measured in the tank, when the volume is large, show rather slight variations among the models. Fig. 3(a) shows results for a tank filled with $3000\,cm^3$ of reaction mixture operating under rather low catalyst concentrations ($0.5\,g\,L^{-1}$). When the recirculation rate is low ($10\,cm^3\,s^{-1}$) there are almost not differences, even with the Perfect Mixing Model (PMM). At higher catalyst concentrations ($2\,g\,L^{-1}$) (Fig. 3(b)) the departure from the PMM

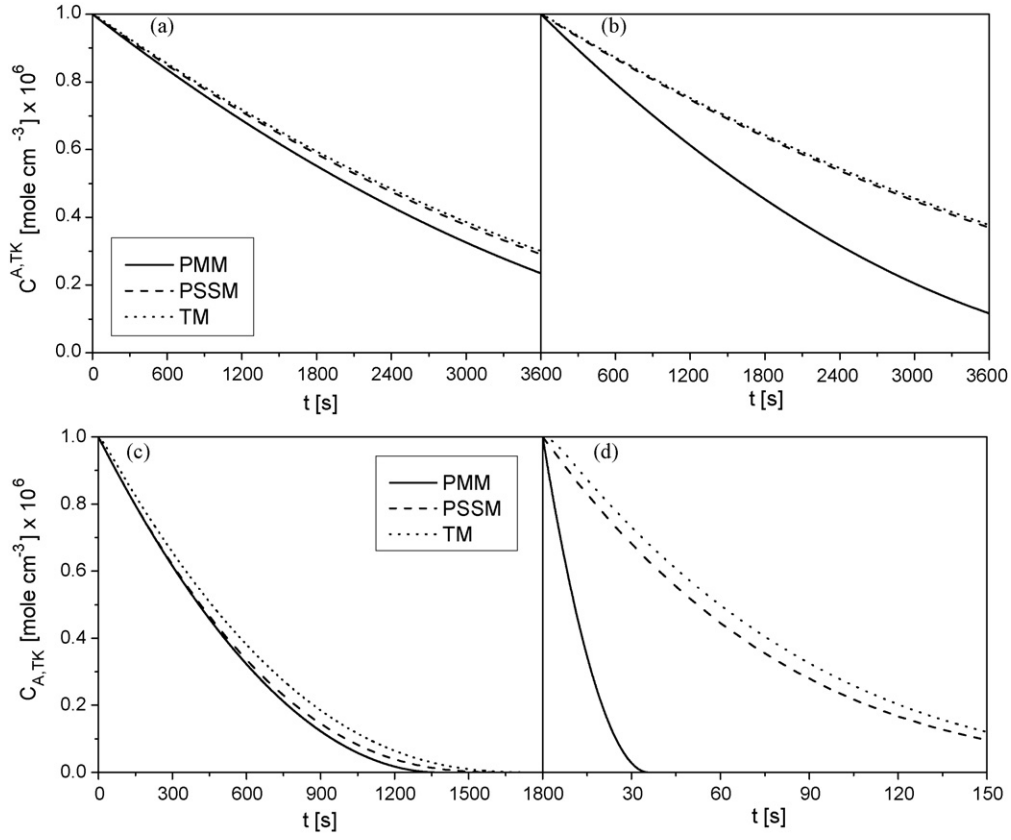

Fig. 3. Comparison of the TM, the PSSM and the PMM models and influence of the damping effect of the tank. 100% irradiation level, $Q = 10\,\mathrm{cm^3\,s^{-1}}$. (a) $C_{mc} = 0.5\,\mathrm{g\,L^{-1}}$, $R_{Het,A} \times 1$, $V_{Tk} = 3000\,\mathrm{cm^3}$. (b) $C_{mc} = 2\,\mathrm{g\,L^{-1}}$, $R_{Het,A} \times 1$, $V_{Tk} = 3000\,\mathrm{cm^3}$. (c) $C_{mc} = 0.5\,\mathrm{g\,L^{-1}}$, $R_{Het,A} \times 1$, $V_{Tk} = 500\,\mathrm{cm^3}$. (d) $C_{mc} = 2\,\mathrm{g\,L^{-1}}$, $R_{Het,A} \times 30$, $V_{Tk} = 500\,\mathrm{cm^3}$.

is noticeable but the differences between the pseudo-stationary state model (PSSM) and the transient model (TM) are almost undistinguishable. In order to show the undisguised differences in the reactor behavior the fluid volume in the tank was reduced to 500 cm^3. Two extreme cases are shown in Fig. 3(c and d). In the first case, with low catalyst concentration and low recirculation rate (well-defined laminar flow with $Re = 221$) the differences between the transient model and the pseudo-stationary state model are more marked but not extremely separated from the PMM. The second case represents a low recirculation rate but much higher catalyst concentration (2 g L^{-1}) and employing a reaction rate that has been virtually increased 30 times (assuming that with a different catalyst the recombination rate of electrons and holes could be reduced significantly). Independently of the very different reaction times (the sort of conditions that one wishes to have in order to apply them in practical reactors) it is shown that the differences between the transient model and the pseudo-stationary state model are not so great but separation from the perfect mixing model (PMM) is remarkable. Varying other operating conditions such as other combinations of catalyst concentrations, flow rates, reaction rates and irradiation rates, results not shown here portrait similar effects: the PSSM always diverge partly from the TM and every time that the change may lead to mass transfer control, as expected, the trivial departure form the PMM condition takes place. The computer processing time between the TM and the PSSM are not very different and from now on all the results will be shown comparing only the TM with the PMM.

4. Results

4.1. Radiation profiles in the bulk

Due to the speed of radiation propagation, the corresponding field of spatial profiles are instantaneously established and are independent of the operating conditions, with the only exception of trivial constituents such as the employed lamps, reactor windows transmittances, filters characteristics – if applicable – and reactor geometrical configuration. In the case of solid photocatalysis, the significant variables for a fixed catalyst brand are the concentration of radiation absorbing species and catalyst particle sizes. For a given device, if the pollutant does not absorb radiation in the operating wavelength range (as it is the case of DCA) the only elements that affect the radiation field are the type and concentration of the catalyst. If the catalyst is mechanically stable and its chemical activity is constant, the radiation balance is independent of time and of the mass balance and the radiation profile for a given type of semiconductor can be calculated, once and for all, as an exclusive function of the catalyst concentration. This assumption has some limitations because the catalyst optical properties are very often affected by the operating pH.

The radiation profiles of the LVRPA ($e^{a}_{\Sigma\lambda}$) as a function of the reactor thickness (y) for different catalyst concentrations confirm, for a different geometry, the general behavior published by Martín et al. [40] and shows that absorption near the reactor windows increases drastically when the catalyst concentration becomes large ($\approx 2\,g\,L^{-1}$) but, at the same time, after no more than 30% of the reactor thickness ($H_R = 1$ cm) the existing absorption is almost negligible because the radiation intensity has been practically fully attenuated. Regarding this last particularity, the opaqueness of the reactor, even for catalyst concentrations as small as $0.5\,g\,L^{-1}$, is almost reached with just 0.5 cm of the path length [51].

4.2. Macroscopic concentration profiles

The radiation field reported above, produces irreducible concentration profiles unless fully turbulent flow conditions are used (see further ahead). Most of them can be conveyed into the unstable intermediate species when their life times are shorter than the characteristic hydrodynamic mixing time. If these significant concentration gradients are transferred to the stable species concentrations, the performance of the reactor will be severely affected; i.e., when these very steep radiation absorption rate gradients exist, the assumption of having a reactor free from stable species concentration gradients will be valid only for very special mixing conditions. We will look at DCA gradients, but similar reasoning can be made for dissolved oxygen; the diffusion coefficients will be slightly larger but the driving force cannot be too large due to its small solubility values. Even more, without replenishing the oxygen concentration in the tank, lack of sufficient oxygen will be a very important difficulty for the reactor operation.

The first useful results can be observed in the concentrations profiles of DCA as a function of the "y"-direction at the reactor exit ($z = L_R$) for two operating conditions under laminar flow ($Q = 10$ and $100\,cm^3\,s^{-1}$). These results agree and complement those published elsewhere [40] remarking in this work the importance of the operating flow rates. These data were obtained employing the 100% irradiation rate and two catalyst concentrations ($C_{mc} = 0.5$ and $2\,g\,L^{-1}$). The equivalent results for $y = 0$ and $y = H_R/2$ are shown in plots of DCA concentration as a function of "z".

Figs. 4 and 5 display these results. In the first set it can be clearly seen that starting from an initial concentration of $1 \times 10^{-6}\,mol\,cm^{-3}$, the DCA concentration falls very dramatically close to the reactor wall of radiation entrance and remain almost unaltered in the center line of the reactor. Even more, for a catalyst concentration of $2\,g\,L^{-1}$ and the lower flow rate, the DCA concentration is practically zero up to a distance of approximately 0.05 cm from the wall ratifying the suspicion of the existence of strong mass transfer limitations. The axial profiles are equally demonstrative of the large differences in the reactor behavior in regions close to the reactor wall and at the center line. For both catalyst concentrations at $y = H_R/2$ the DCA concentration is almost unaltered along the whole reactor length. On the contrary, the plot shows significant changes at $y = 0$. Furthermore, with $2\,g\,L^{-1}$ of catalyst

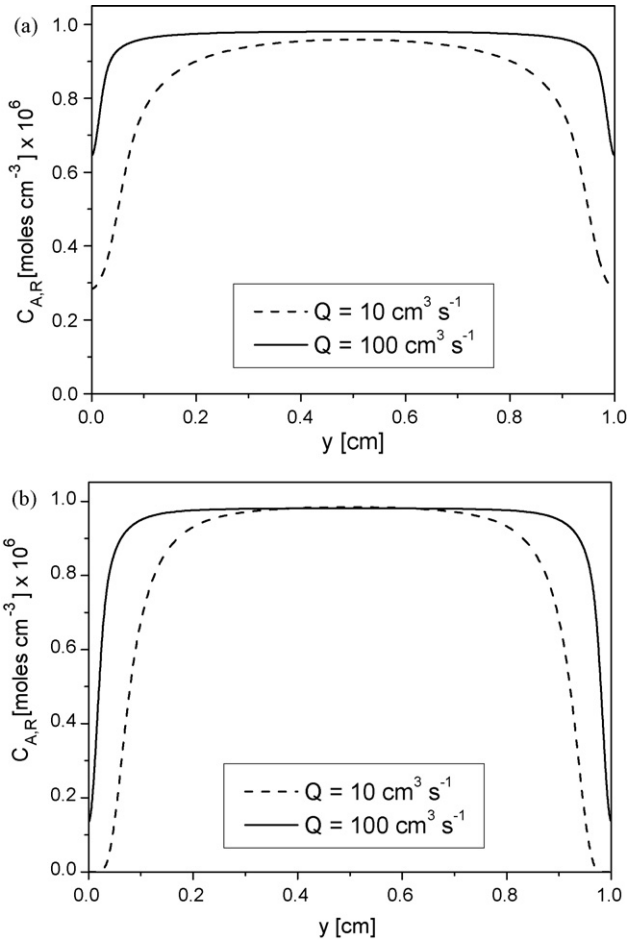

Fig. 4. Concentration profiles of reactant A inside the reactor as a function of y. $z = L_R$, 100% irradiation level, $R_{Het,A} \times 1$, $V_{Tk} = 3000\,cm^3$, $t = 60$ s. (a) $C_{mc} = 0.5\,g\,L^{-1}$. (b) $C_{mc} = 2\,g\,L^{-1}$.

concentration and the lower flow rate, the DCA concentration at $y = 0$ is almost 0 after 3.5 cm of the photoreactor length. The effects of the employed flow rate are again clearly remarked.

4.3. Effect of the catalyst concentration and irradiation rates

This effect is better analyzed if, in a first instance, it is examined under the ideal condition of a perfectly mixed reactor. Under these conditions no bulk concentration profiles should exist. Fig. 6(a) shows that the final concentration presents a monotonous increase in the reactor performance when the catalyst concentration is increased even much beyond the point where, from the radiation point of view, an important volume of the reactor is almost not irradiated. This is evidence that a catalytic effect (more surface area, or more active sites) also affect the rate, surpassing the instinctive interpretation that the limitation is due to the length of the light penetration. It is clear that the well mixed reactor displays the best performance. Employing the TM, at very high flow rates under turbulent flow ($Q = 1000\,cm^3\,s^{-1}$; $Re = 22{,}140$), results not shown here indicate that the performance is almost undistinguishable equal.

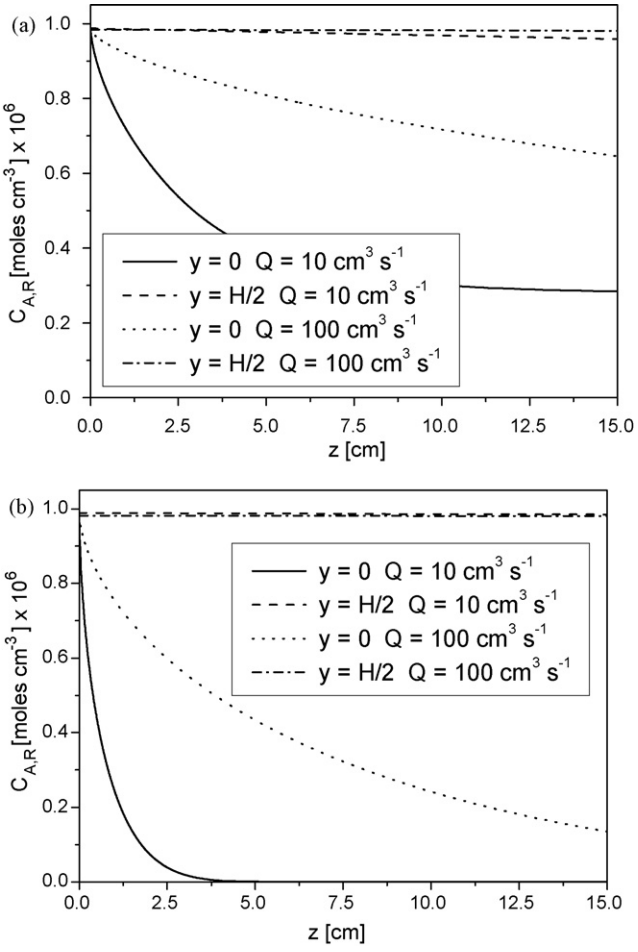

Fig. 5. Concentration profiles of reactant A inside the reactor as a function of z. 100% irradiation level, $R_{Het,A} \times 1$, $V_{Tk} = 3000\,cm^3$, $t = 60\,s$. (a) $C_{mc} = 0.5\,g\,L^{-1}$. (b) $C_{mc} = 2\,g\,L^{-1}$.

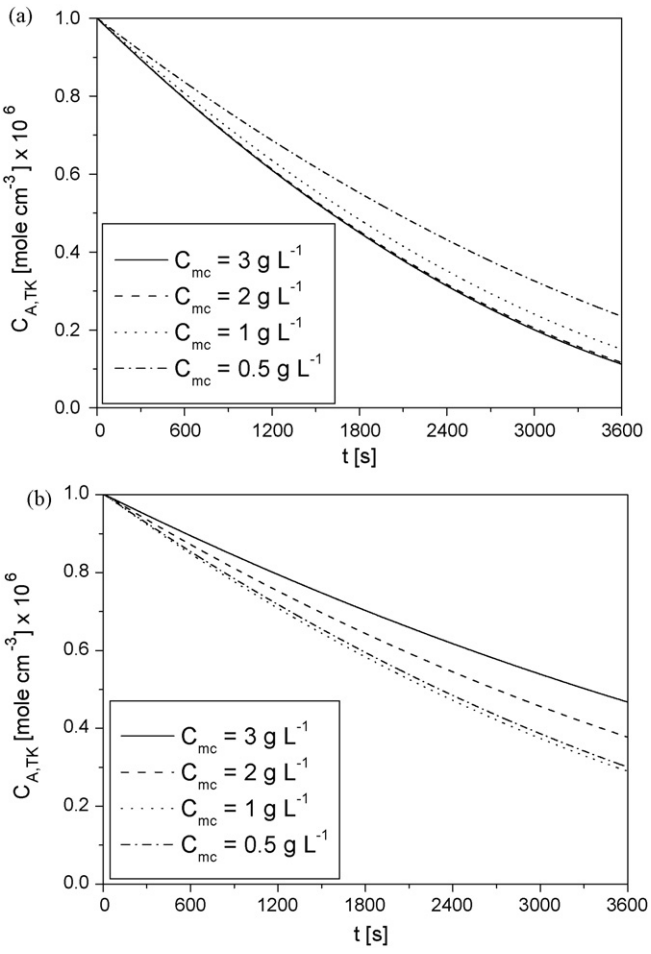

Fig. 6. Effect of catalyst concentration. 100% irradiation level, $R_{Het,A} \times 1$, $V_{Tk} = 3000\,cm^3$. (a) PMM. (b) TM, $Q = 10\,cm^3\,s^{-1}$.

Two effects contribute to this result: (i) a different velocity profile is present and (ii) the eddy diffusion coefficient is about five orders of magnitude larger than the molecular one and the concentration profiles are almost flat with the exception of regions close to the reactor walls (see Fig. 7). However, in Fig. 6(b) made with $Q = 10\,cm^3\,s^{-1}$, it is shown that when the catalyst loading is increased and mixing in the y-direction is not so strong, the previously observed trend in Fig. 6(a) is interrupted. Employing the TM, the performance of the reactor at catalyst concentrations from 0.5 to $3\,g\,L^{-1}$ is even less efficient (recall that $0.5\,g\,L^{-1}$ turns the reactor almost opaque from $y = 0.3$ to 0.7 cm). Thus, the conclusion is that larger catalyst concentrations offer to the reaction more active sites till the point where the substantial absence of light and the absence of strong mixing in the y-direction permit that diffusive limitations overcome the previously quoted beneficial effect.

A very evident observation is obtained comparing initial changes in concentration in the tank, employing the two models, as a function of the catalyst concentration for different flow rates (including the case of $1000\,cm^3\,s^{-1}$ in the frank turbulent flow, with the velocity profile derived for this regime and the corresponding eddy diffusion coefficient in the mass balance).

In Fig. 8(a and b) the results are shown for 100% of irradiation rates and for an irradiation rate reduced with neutral filters to 10% of the original one. In Fig. 8(a) the PMM does not shows any special particularity but with the TM for all flow rates below $1000\,cm^3\,s^{-1}$ and all catalyst concentrations, the initial rates go

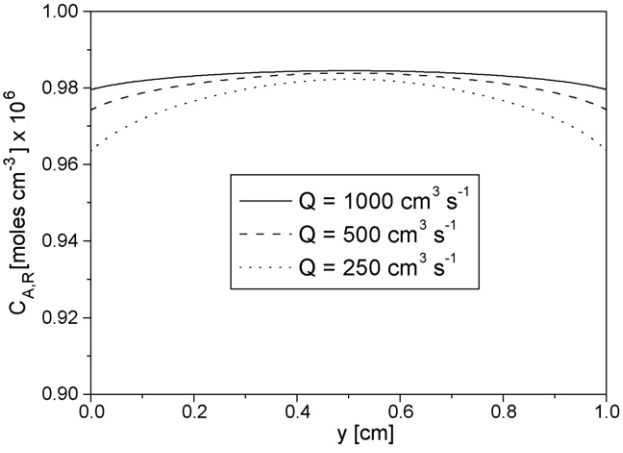

Fig. 7. Concentration profiles for reactant A under very high recirculating flow rates but high catalyst concentration and high irradiation rates. $z = L_R$, 200% irradiation level, $C_{mc} = 3\,g\,L^{-1}$, $R_{Het,A} \times 1$, $V_{Tk} = 3000\,cm^3$, $t = 60\,s$.

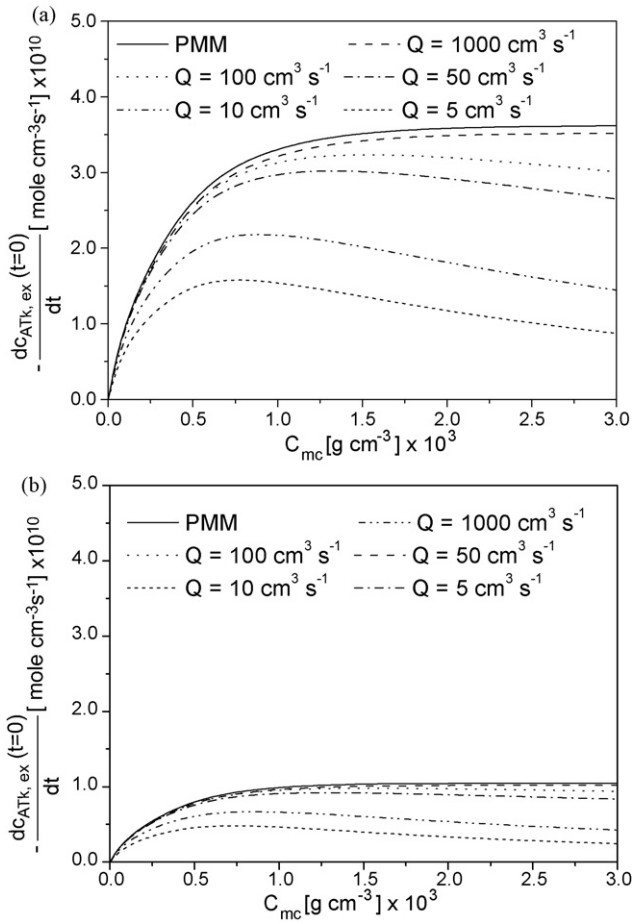

Fig. 8. (a) Initial rates in the tank as a function of the catalyst concentration for different recirculation flow rates. $R_{Het,A} \times 1$, $V_{Tk} = 3000\,cm^3$. (a) 100% irradiation level. (b) 10% irradiation level.

to a maximum ($Q = 100\,cm^3\,s^{-1}$, maximum at $C_{mc} \cong 1.5\,g\,L^{-1}$; for $Q = 10\,cm^3\,s^{-1}$ at $C_{mc} \cong 1\,g\,L^{-1}$, and for $Q = 5\,cm^3\,s^{-1}$ at $C_{mc} \cong 0.5\,g\,L^{-1}$) and then decrease.

The effect of the catalyst concentration combined with variations in the irradiation rates is also important. For example, Fig. 9(a) shows results for the best conditions to avoid mass transfer resistances. The concentration in the tank is almost undistinguishable from perfect mixing and three different flow rates, when the catalyst concentration is $0.5\,g\,L^{-1}$ and the irradiation rate is 10% of the original. Under the same conditions, but for a catalyst concentration of $3\,g\,L^{-1}$, Fig. 9(b) indicates significant deviations resulting from the strong differences in light penetration into the reactor and the existence of very important concentration gradients that, only with a fully developed turbulent flow (with $Re = 22{,}140$ and the corresponding velocity profiles and mass transfer equations) and the presence of more active sites, can compensate the limitations introduced by the radiation field.

In this respect, the most critical operation from the kinetic control point of view corresponds to the case of a virtual 200% increase in the original irradiation rate and a catalyst loading of $3\,g\,L^{-1}$. The differences are very noticeable with the exception at very high flow rates. It must be noted that for very high flow rates, the reactor most surely works under differential operating conditions thus approaching even more the PMM. This is supported by Fig. 10 for the same operating conditions and a reaction rate virtually increased 30 times with the assumption that, maintaining all other variables constant, with a different catalyst, the recombination of electrons and holes can be greatly reduced. Here, it is seen that even for $Re = 22{,}140$, a slight separation from the PMM starts to be visible. It is then clear that for very high irradiation rates and large catalyst concentrations only strong mixing conditions in the characteristic direction of radiation propagation (recall Fig. 7) can avoid mass transfer limitations.

The case of high irradiation rates as introduced in the above discussion, also deserves some considerations. It has been reported [42,75,76] that increasing irradiation rates to the point where the reaction rate could take on very high values results in a zero order dependence with respect to the LVRPA. The proposed explanation is a total depletion of DCA on the surface of the catalyst or in its very close surroundings. Employing a rather low catalyst concentration ($0.5\,g\,L^{-1}$) and choosing the flow rate as a parameter, it is possible to compare the changes in the concentration of the tank at two very different irradiation rates: 10 and 200% of the originally adopted irradiation level (Figs. 9(a) and 11). In the first case the data are about the same for all flow rates and the PMM, in spite of the fact that the initial rates show some differences at the beginning of the run. In the second case the discrepancies are more apparent, indicating that in regions where the incident radiation is very high there is an important consumption of DCA leading to a mass transfer limitation in the reaction rate, particularly at the lowest flow rates. Thus, one can conclude that very high irradiation rates can also produce an operation under diffusive control. It is fair to note that strong irradiation rates with lamps above 40–50 W of nominal input power are seldom used in photocatalytic studies and applications.

A sort of summary of these simulations can be commented recalling Fig. 7. It shows reactor concentrations at $z = L_R$ after 60 s of operation, when the catalyst concentration is $3\,g\,L^{-1}$, the irradiation level is 200%, the flow rate is 250, 500 and $1000\,cm^3\,s^{-1}$ where turbulent velocity profile and eddy diffusivity have been assumed: concentration gradients very close to the windows of irradiation are still significant. This figure shows that the effect of high irradiation rates and high catalyst concentrations may even distort the turbulent flow concentration profiles in regions close to the reactor wall and, rigorously speaking, concentration gradients in the reactor cannot be fully avoided. Under the same conditions as discussed above, for the concentration measured in the tank, only the turbulent flow in the reactor resulting for a flow rate of $1000\,cm^3\,s^{-1}$ ($Re = 22{,}140$) permits to approach very closely the behavior of the perfectly mixed photocatalytic reactor. The consideration that, in addition, this may be a disguised result produced by the dilution in the tank volume, mainly because the reactor in practice could be operating under differential concentration conditions, cannot be avoided. The existence of concentration gradients in the reactor, under high catalyst loadings and strong illumination, even under differential operation and strong turbulent

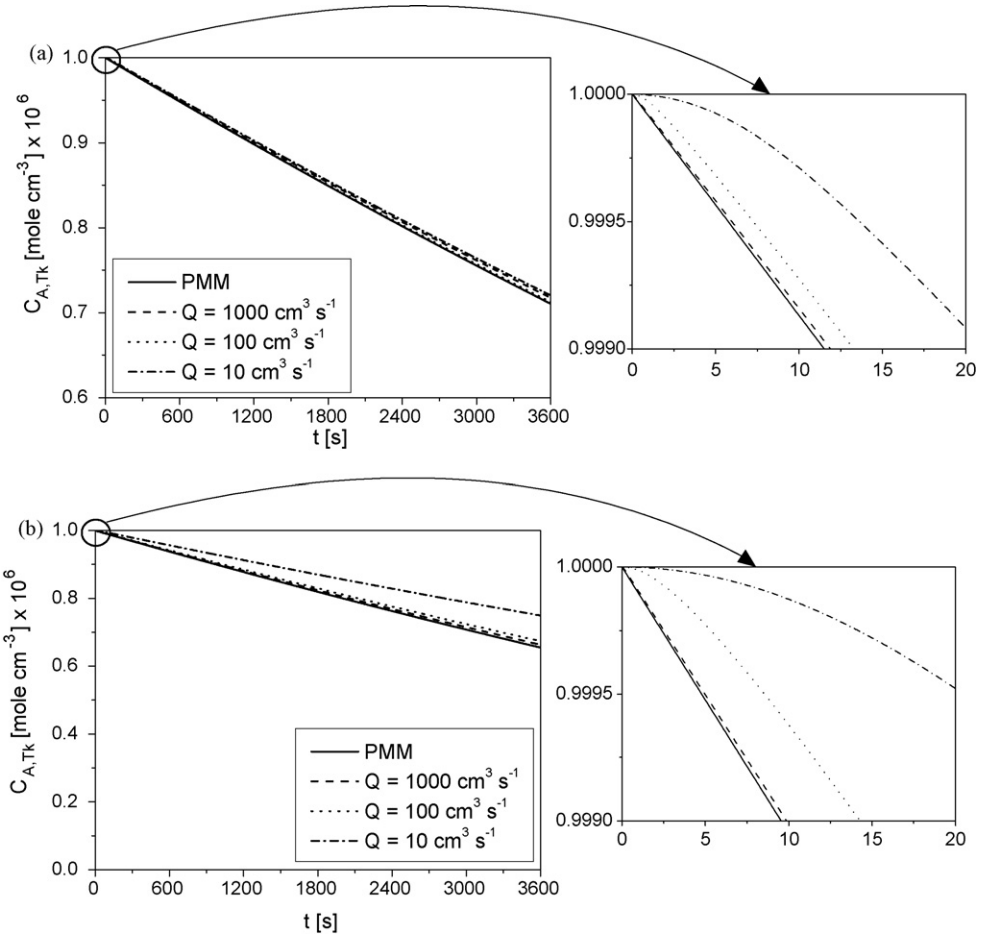

Fig. 9. Effect of catalyst concentration at low irradiation level. 10% irradiation level, $R_{Het,A} \times 1$, $V_{Tk} = 3000\,cm^3$. (a) $C_{mc} = 0.5\,g\,L^{-1}$. (b) $C_{mc} = 3\,g\,L^{-1}$.

flow conditions up to the point explored in this work, cannot permit to say that mass transport limitations have been 100% avoided.

The observations made in the last paragraph concerning the possibility of disguising some of the results calculated for the concentrations measured in the tank due to a possible differential operation in the reactor, led us to a last set of virtual experiments. A new virtual change in the reactor configuration has been made, extending its length to $L_R = 80\,cm$. Consider the pivoting conditions discussed above in Fig. 9(a) (catalyst concentration of $0.5\,g\,L^{-1}$ and irradiation level of 10% of the original). It was said that that under these conditions we have always an almost kinetically controlled regime. The situation changed in Fig. 11 due to the effect produced by the drastically change in the irradiation level. Now, under the same operating conditions but with a reactor that has an illuminated length of 80 cm it is possible

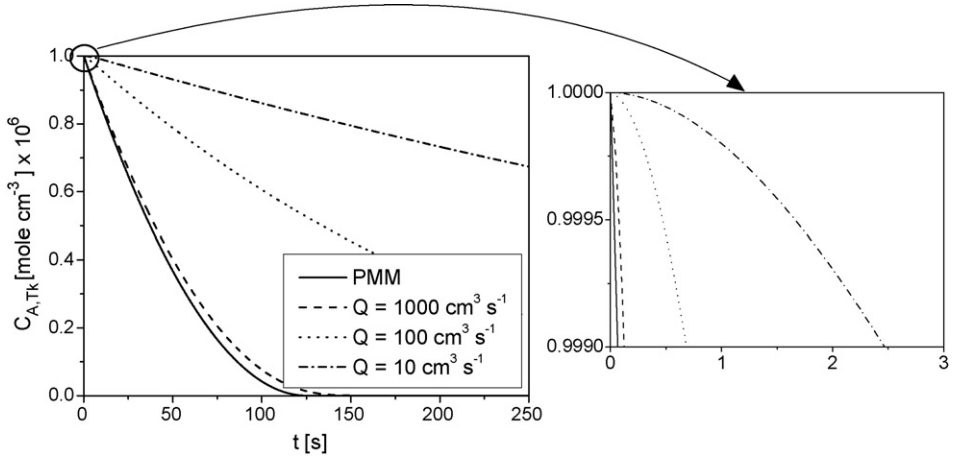

Fig. 10. Effect of virtual changes in the reaction rates at high irradiation level. 200% irradiation level, $C_{mc} = 3\,g\,L^{-1}$, $R_{Het,A} \times 30$, $V_{Tk} = 3000\,cm^3$.

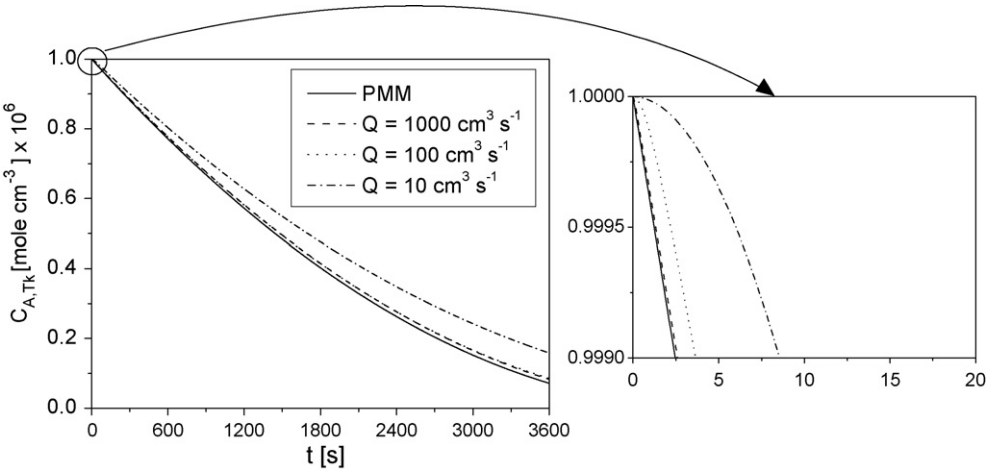

Fig. 11. Effects of the irradiation rates. 200% irradiation level, $C_{mc} = 0.5\,g\,L^{-1}$, $R_{Het,A} \times 1$, $V_{Tk} = 3000\,cm^3$.

to see that in the previously commented results, concentrations measured in the tank were, to some extent, disguised by the almost differential operation of the reactor (Fig. 12(a)). Intense recirculation rates are needed to approach the PMM behavior. Moving the catalyst concentration up to $3\,g\,L^{-1}$, employing the 200% irradiation level, increasing in a virtual manner the reaction rate 30 times and using the reactor illuminated length of 80 cm an important change is observed (Fig. 12(b)). Clearly, the operation of the reactor may be in a regime of strong concentration gradients and only the case of recirculation rates as high as $1000\,cm^3\,s^{-1}$, permits to approach the PMM. Thus, a careful selection of the operating conditions must be performed to make

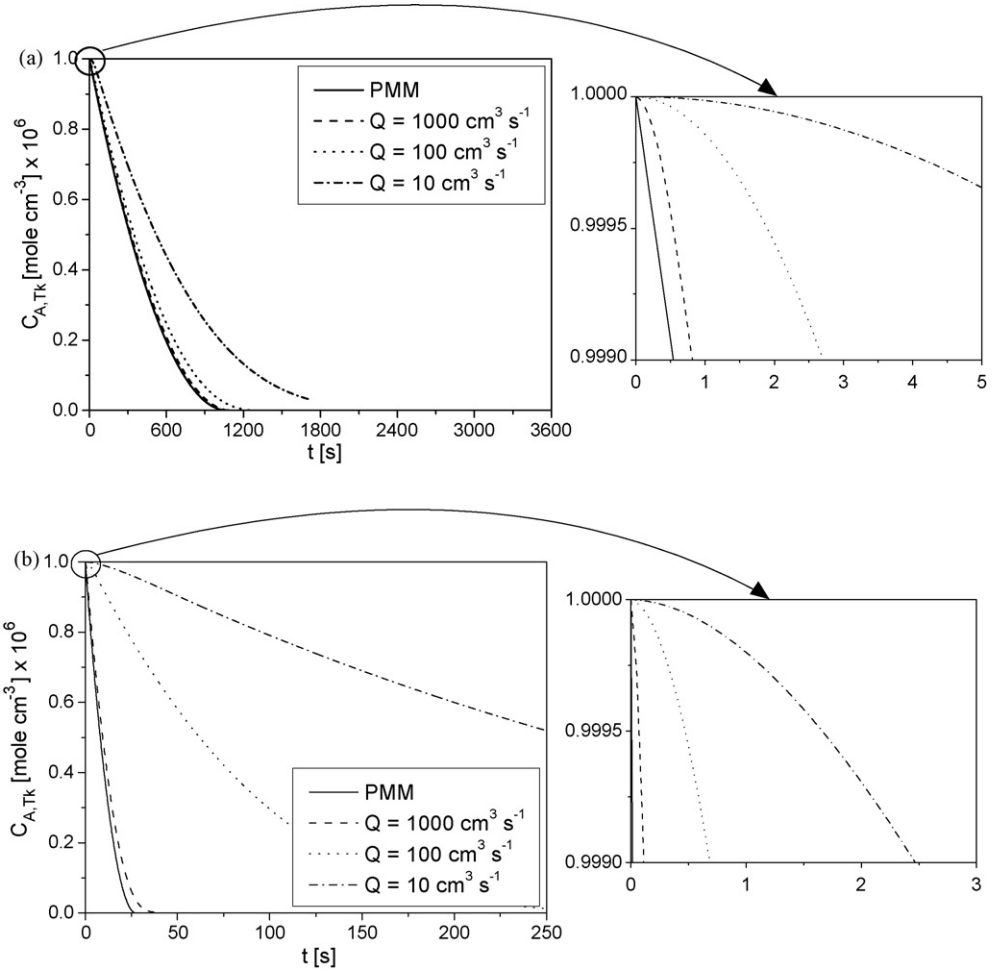

Fig. 12. A virtual operation with a reactor having an illuminated length of 80 cm. 200% irradiation level, $V_{Tk} = 3000\,cm^3$. (a) $C_{mc} = 0.5\,g\,L^{-1}$, $R_{Het,A} \times 1$. (b) $C_{mc} = 3\,g\,L^{-1}$, $R_{Het,A} \times 30$.

sure that in laboratory reactors the observed results correspond to a kinetically controlled regime.

In Figs. 9–12 an amplification of the first few seconds of the reaction time clearly shows the particular behavior of the flow reactor during the first mean residence time which is magnified at the lower recirculation rates.

These results are very useful to call the attention of many kinetic reports in the literature that are said to have been obtained under perfectly mixing conditions. With an usually irreducible non-uniformity in the radiation field and the use of rather large catalyst concentrations (that have very high radiation absorption properties) the achievement of very strong mixing conditions is mandatory if simple mass balance equations are used to interpret the experimental results.

5. Conclusions

The possibility of mass transport limitations in the bulk of photocatalytic suspensions of pure titanium dioxide have been analyzed in a detailed study based on fundamental principles and a realistic kinetics derived from a complete reaction mechanisms. The most important conclusion is that concentration profiles in the bulk will be always present unless very good mixing conditions in the characteristic direction of radiation propagation are used.

If concentration gradients are present, they can produce mass transport limitations in the bulk. Moreover, they will make the assumption of perfect mixing conditions in the usually employed mass balances an incorrect hypothesis.

The combination of high irradiation rates with high catalyst loading should be used with great care, particularly if the reaction kinetics is not known, because mass transfer limitations may be present.

In flow reactors, when fully developed turbulent flow operation is achieved, these mass transfer limitations are almost negligible.

When the photocatalytic reaction is not fast (which is common in water environments), employing TiO_2 mass concentrations below $1\,g\,L^{-1}$, incoming irradiation rates below 1.0×10^{-7} Einstein $cm^{-2}\,s^{-1}$ and very good mixing conditions, it will be safe to assume that mass transport limitations in the bulk of slurry photocatalytic reactors are not important.

Acknowledgements

Thanks are given to Universidad Nacional del Litoral, CONICET and Agencia Nacional de Promoción Científica y Tecnológica for financial help and the doctoral fellowship of MMB. The invaluable help of Doctor Jorge D'Elia and the technical assistance of Eng. Claudia Romani is gratefully appreciated. Computer simulations have been performed in the Aquiles Beowulf Cluster at Centro Internacional de Métodos Computacionales en Ingeniería, CIMEC (CONICET-UNL). Aquiles cluster was built with grant (PME 209/2003) from Agencia Nacional de Promoción Científica y Tecnológica and CONICET.

Appendix A

From the kinetic scheme presented in Table 2 [53], the reaction rate of the initiation step, assuming a local superficial rate of photon absorption (LSRPA) with an average primary quantum yield, is:

$$R_{\mathrm{Het},0} = R_{\mathrm{Het,g}} = \int_\lambda \Phi_\lambda e^{\mathrm{a}}_{\mathrm{S},\lambda}\,\mathrm{d}\lambda = \bar{\Phi}_\lambda \int_\lambda e^{\mathrm{a}}_{\mathrm{S},\lambda}\,\mathrm{d}\lambda \tag{A.1}$$

Where the definition of a LSRPA averaged primary quantum yield as:

$$\bar{\Phi}_\lambda = \frac{\int_\lambda \Phi_\lambda e^{\mathrm{a}}_{\mathrm{S},\lambda}\,\mathrm{d}\lambda}{\int_\lambda e^{\mathrm{a}}_{\mathrm{S},\lambda}\,\mathrm{d}\lambda} \tag{A.2}$$

The heterogeneous reaction rate of DCA degradation is:

$$\begin{aligned} R_{\mathrm{Het,DCA^-}} &= -R_{\mathrm{Het},2} = -k_2 C_{\mathrm{DCA^-_{ads}}} C_{\mathrm{h^+}} \\ &= -k_2 K_1 C_{\mathrm{sites}} C_{\mathrm{DCA^-}} C_{\mathrm{h^+}} \end{aligned} \tag{A.3}$$

With:

$$C_{\mathrm{DCA^-_{ads}}} = K_1 C_{\mathrm{sites}} C_{\mathrm{DCA^-}} \tag{A.4}$$

Considering that the rate of formation of unstable intermediates is equal to the rate of disappearance:

$$\begin{aligned} R_{\mathrm{Het,h^+}} &= R_{\mathrm{Het},0} - R_{\mathrm{Het},2} - R_{\mathrm{Het},8} \\ &= R_{\mathrm{Het,g}} - k_2 K_1 C_{\mathrm{sites}} C_{\mathrm{DCA^-}} C_{\mathrm{h^+}} - k_8 C_{\mathrm{e^-}} C_{\mathrm{h^+}} \\ &= 0 \end{aligned} \tag{A.5}$$

Solving for $C_{\mathrm{h^+}}$:

$$C_{\mathrm{h^+}} = \frac{R_{\mathrm{Het,g}}}{k_2 K_1 C_{\mathrm{sites}} C_{\mathrm{DCA^-}} - k_8 C_{\mathrm{e^-}}} \tag{A.6}$$

In the same way one can obtain the concentrations of $C_{\mathrm{e^-}}$, $C_{\mathrm{HO_2^\bullet}}$ and $C_{\mathrm{O_2^{\bullet-}}}$.

The hole and electron concentrations, after some algebra, result:

$$C_{\mathrm{e^-}} = \frac{R_{\mathrm{Het,g}}}{k_8 C_{\mathrm{h^+}} + 2k_9 K_4 C_{\mathrm{sites}} C_{\mathrm{O_2}}} \tag{A.7}$$

$$\begin{aligned} C_{\mathrm{h^+}} = {} & \left(\frac{1}{k_2 K_1 k_8 C_{\mathrm{sites}} C_{\mathrm{DCA^-}}}\right) \\ & \times \Big\{ -k_2 K_1 k_9 K_4 C^2_{\mathrm{sites}} C_{\mathrm{DCA^-}} C_{\mathrm{O_2}} \\ & + [(k_2 K_1 k_9 K_4 C^2_{\mathrm{sites}} C_{\mathrm{DCA^-}} C_{\mathrm{O_2}})^2 \\ & + 2k_2 K_1 k_8 k_9 K_4 C^2_{\mathrm{sites}} R_{\mathrm{Het,g}} C_{\mathrm{DCA^-}} C_{\mathrm{O_2}}]^{1/2} \Big\} \end{aligned} \tag{A.8}$$

After substitution of the superficial rate of electron–hole generation and including the values of $C_{\mathrm{h^+}}$ and $C_{\mathrm{e^-}}$:

$$R_{\mathrm{Het,DCA^-}} = \left(\frac{1}{k_8}\right)\left\{k_2K_1k_9K_4C_{\mathrm{sites}}^2C_{\mathrm{DCA^-}}C_{\mathrm{O_2}} - \left[\left(k_2K_1k_9K_4C_{\mathrm{sites}}^2C_{\mathrm{DCA^-}}C_{\mathrm{O_2}}\right)^2 + 2k_2K_1k_8k_9K_4C_{\mathrm{sites}}^2C_{\mathrm{DCA^-}}C_{\mathrm{O_2}}\bar{\Phi}_\lambda\int_\lambda e^{\mathrm{a}}_{\mathrm{S},\lambda}\,\mathrm{d}\lambda\right]^{1/2}\right\} \quad (A.9)$$

Defining:

$$\alpha_1 = \frac{k_2K_1k_9K_4C_{\mathrm{sites}}^2}{k_8} \quad \text{and}$$

$$\alpha_2 = \frac{k_2K_1k_9K_4C_{\mathrm{site}}^2\bar{\Phi}_\lambda}{k_8} \quad (A.10)$$

The degradation rate per unit particle surface area results:

$$R_{\mathrm{Het,DCA^-}} = \alpha_1C_{\mathrm{DCA^-}}C_{\mathrm{O_2}} - \sqrt{\left(\alpha_1C_{\mathrm{DCA^-}}C_{\mathrm{O_2}}\right)^2 + 2\alpha_2C_{\mathrm{DCA^-}}C_{\mathrm{O_2}}\int_\lambda e^{\mathrm{a}}_{\mathrm{S},\lambda}\,\mathrm{d}\lambda} \quad (A.11)$$

Introducing the local volumetric rate of photon absorption the reaction rate per unit suspension volume is:

$$a_{\mathrm{V}}R_{\mathrm{Het,DCA^-}} = S_{\mathrm{g}}C_{\mathrm{mc}}\left\{\alpha_1C_{\mathrm{DCA^-}}C_{\mathrm{O_2}} - \sqrt{\left(\alpha_1C_{\mathrm{DCA^-}}C_{\mathrm{O_2}}\right)^2 + 2\frac{\alpha_2C_{\mathrm{DCA^-}}C_{\mathrm{O_2}}\int_\lambda e^{\mathrm{a}}_\lambda\,\mathrm{d}\lambda}{S_{\mathrm{g}}C_{\mathrm{mc}}}}\right\} \quad (A.12)$$

The kinetic parameters α_1 and α_2 were recalculated from the original data of Zalazar [54], obtaining the following values:

$$\alpha_1 = 2.35 \pm 0.42\,\mathrm{cm^4\,mol^{-1}\,s^{-1}} \quad \text{and}$$

$$\alpha_2 = 1.25 \pm 0.41\,\mathrm{cm^4\,s^{-1}\,Einstein^{-1}}. \quad (A.13)$$

References

[1] R.W. Matthews, Photo-oxidation of organic material in aqueous suspensions of titanium dioxide, Water Res. 20 (5) (1986) 569– 578.

[2] R.W. Matthews, Environment: photochemical and photocatalytic processes. degradation of organic compounds, in: E. Pelizzetti, M. Schiavello (Eds.), Photochemical Conversion and Storage of Solar Energy, Kluwer Academic Publishers, Netherlands, 1991, pp. 427–449.

[3] D.F. Ollis, E. Pellizzetti, Destruction of water contaminants, Environ. Sci. Technol. 25 (9) (1991) 1523–1529.

[4] G. Goutailler, J.C. Valette, C. Guillard, O. Païssé, R. Faure, Photocatalyzed degradation of cyromazine in aqueous titanium dioxide suspensions: comparison with photolysis, J. Photochem. Photobiol. A: Chem. 141 (2001) 79–84.

[5] A. Topalov, D. Molnar-Gabor, J. Csanadi, Photocatalytic oxidation of the fungicide metalaxyl dissolved in water over TiO_2, Water Res. 33 (1999) 1371–1376.

[6] G. Li Puma, J.N. Khor, A. Brucato, Modeling of an annular photocatalytic reactor for water purification: oxidation of pesticides, Environ. Sci. Technol. 38 (2004) 3737–3745.

[7] D. Chen, A.K. Ray, Phtodegradation kinetics of 4-nitrophenol in TiO_2 suspension, Water Res. 32 (1998) 3223–3234.

[8] D. Chen, A.K. Ray, Photocatalytic kinetics of phenol and its derivatives over UV irradiated TiO_2, Appl. Catal. B: Environ. 23 (1999) 143–157.

[9] A. Sobczynski, L. Duczmal, W. Zmudzinski, Phenol destruction by photocatalysis on TiO_2: an attempt to solve the reaction mechanism, J. Mol. Catal. A: Chem. 213 (2004) 225–230.

[10] S. Ahmed, D. Ollis, Solar photoassisted catalytic decomposition of the chlorinated hydrocarbons trichloroethylene and trichloromethane, Sol. Energy 32 (5) (1984) 597–601.

[11] P.C. Calza, C. Minero, A. Hiskia, E. Papaconstantinou, E. Pelizzetti, Photocatalytic transformations of CCl_3Br, CBr_3F, $CHCl_2Br$ and CH_2BrCl in aerobic and anaerobic conditions, Appl. Catal. B: Environ. 29 (2001) 23–34.

[12] U. Stafford, K. Gray, P.V. Kamat, Photocatalytic degradation of 4-chlorophenol: the effects of varying TIO_2 concentration and light wavelength, J. Catal. 167 (1997) 25–35.

[13] J. Chen, D.F. Ollis, W.H. Rulkens, H. Bruning, Photocatalyzed oxidation of alcohols and organochlorides in the presence of native TiO_2 and metallized TiO_2 suspensions. Part (II): photocatalytic mechanisms, Water Res. 33 (1999) 669–676.

[14] A. Chemseddine, H.P. Boehm, A study of the primary step in the photochemical degradation of acetic acid and chloroacetic acids on a TiO_2 photocatalyst, J. Mol. Catal. 60 (1990) 295–311.

[15] Y. Îinel, A.N. Ökte, Photocatalytic degradation of malonic acid in aqueous suspensions of titanium dioxide: an initial kinetic investigation of CO_2 photogeneration, J. Photochem. Photobiol. A: Chem. 96 (1996) 175–180.

[16] M.F.J. Dijkstra, H.J. Panneman, J.G.M. Winkelman, J.J. Kelly, A.A.C.M. Beenackers, Modeling the photocatalytic degradation of formic acid in a reactor with immobilized catalyst, Chem. Eng. Sci. 57 (2002) 4895–4907.

[17] A.K. Ray, A.A.C.M. Beenackers, Novel swirl flow reactor for kinetic studies of semiconductor photocatalysis, AIChE J. 43 (10) (1997) 2571–2578.

[18] V. Subramanian, P.V. Kamat, E.E. Wolf, Mass transfer and kinetic studies during the photocatalytic degradation of an azo dye on optically transparent electrode thin film, Ind. Eng. Chem. Res. 42 (2003) 2131–2138.

[19] M.R. Hoffmann, S.T. Martin, W. Choi, D.W. Bahnemann, Environmental applications of semiconductor photocatalysis, Chem. Rev. 95 (1995) 69–96.

[20] R.L. Pozzo, M.A. Baltanás, A.E. Cassano, Towards a precise assessment of the performance of supported photocatalysts for water detoxification processes, Catal. Today 54 (1999) 143–157.

[21] R.L. Pozzo, J.L. Giombi, M.A. Baltanás, A.E. Cassano, The performance in a fluidized bed reactor of photocatalysts immobilized onto inert supports, Catal. Today 62 (2000) 175–187.

[22] R.L. Pozzo, J.L. Giombi, M.A. Baltanás, A.E. Cassano, Radiation extinction of slurried TiO_2 as a function of mechanical action and ionic composition of the suspending media: a key factor in the photocatalytic efficiency, Appl. Catal. B: Environ. 38 (2002) 61–69.

[23] M.F.J. Dijkstra, A. Michorius, H.J. Panneman, A.A.C.M. Beenackers, Development of a continuous photocatalytic reactor, in: Slurry versus Immobilized, Conference Proceedings Hungarian Journal of Industrial Chemistry, vol. 1, 1999, pp. 15–17.

[24] M.F.J. Dijkstra, H. Buwalda, A.W.F. de Jong, A. Michorius, J.G.M. Winkelman, A.A.C.M. Beenackers, Experimental comparison of three reactor designs for photocatalytic water purification, Chem. Eng. Sci. 56 (2001) 547–555.

[25] A.E. Cassano, O.M. Alfano, Reaction engineering of suspended solid heterogeneous photocatalytic reactors, Catal. Today 58 (2000) 167–197.

[26] M.F.J. Dijkstra, E.C.B. Koerts, A.A.C.M. Beenackers, L.A. Wesselingh, Performance of immobilized photocatalytic reactors in continuous mode, AIChE J. 49 (3) (2003) 734–744.

[27] D. Chen, F. Li, A.K. Ray, Effect of mass transfer and catalyst layer thickness on photocatalytic reaction, AIChE J. 46 (5) (2000) 1034–1045.

[28] D. Chen, F. Li, A.K. Ray, External and internal mass transfer effect on photocatalytic degradation, Catal. Today 66 (2001) 475–485.

[29] R.L. Pozzo, M.A. Baltanás, A.E. Cassano, Supported titanium oxide as photocatalyst in water decontamination: state of the art, Catal. Today 39 (1997) 219–231.
[30] R.L. Pozzo, R.J. Brandi, J.L. Giombi, M.A. Baltanás, A.E. Cassano, Design of fluidized bed photoreactors: optical properties of photocatalytic composites of titania CVD-coated onto quartz sand, Chem. Eng. Sci. 60 (2005) 2785–2794.
[31] R.L. Pozzo, R.J. Brandi, J.L. Giombi, A.E. Cassano, M.A. Baltanás, Fluidized bed photoreactors using composites of titania CVD-coated onto quartz sand as photocatalyst: assessment of photochemical efficiency, Chem. Eng. J. 118 (2006) 153–159.
[32] C.S. Turchi, D.F. Ollis, Photocatalytic reactor design: an example of mass transfer limitations with an immobilized, Catal. J. Phys. Chem. 92 (1988) 6852–6853.
[33] A. Sclafani, A. Brucato, L. Rizzuti, Mass transfer limitation in a packed bed photoreactor used for phenol removal, in: D.F. Ollis, H. Al-Ekabi (Eds.), Photocatalytic Purification and Treatment of Water and Air, Elsevier, Amsterdam, 1993, pp. 533–545.
[34] M.E. Edwards, C.M. Villa, C.G. Hill, T.W. Chapman, Effectiveness factor for photocatalytic reactions occurring in planar membranes, Ind. Eng. Chem. Res. 35 (1996) 712–720.
[35] D.D. Dionysiou, M.T. Suidan, I. Baudin, J.M. Laîné, Oxidation of organic contaminants in a rotating disk photocatalytic reactor: reaction kinetic in the liquid phase and the role of mass transfer based on the dimensionless Damköhler number, Appl. Catal. B: Environ. 38 (2002) 1–16.
[36] S. Zhou, A.K. Ray, Kinetic studies for photocatalytic degradation of eosin b on a thin film of titanium dioxide, Ind. Eng. Chem. Res. 42 (2003) 6033–6620.
[37] M.F.J. Dijkstra, A. Michorius, H. Buwalda, H.J. Panneman, J.G.M. Winkelman, A.A.C.M. Beenackers, Comparison of the efficiency of immobilized and suspended systems in photocatalytic degradation, Catal. Today 66 (2001) 487–494.
[38] M. Bideau, B. Claudel, L. Faure, H. Kazouan, Diffusional limitations in liquid phase photocatalysis, Prog. React. Kinet. 19 (1994) 195–209.
[39] K. Mehrotra, G.S. Yablonsky, A.K. Ray, Kinetic studies of photocatalytic degradation in a TiO_2 slurry system: distinguishing working regimes and determining rate dependences, Ind. Eng. Chem. Res. 42 (2003) 2273–2281.
[40] C.A. Martín, G. Camera-Roda, F. Santarelli, Effective design of photocatalytic reactors: influence of radiative transfer on their performance, Catal. Today 48 (1999) 307–313.
[41] N. Serpone, Relative photonic efficiencies and quantum yields in heterogeneous photocatalysis, J. Photochem. Photobiol. A: Chem. 104 (1997) 1–12.
[42] C.S. Turchi, D.F. Ollis, Mixed reactant photocatalysis: intermediates and mutual rate inhibition, J. Catal. 119 (1989) 483–496.
[43] T.Y. Wei, C.C. Wan, Heterogeneous photocatalytic oxidation of phenol with titanium dioxide powders, Ind. Eng. Chem. Res. 30 (1991) 1293– 1300.
[44] A. Salinaro, N. Serpone, Terminology relative photonic efficiencies and quantum yields in heterogeneous photocatalysis. Part II: experimental determination of quantum yields, Pure Appl. Chem. 71 (2) (1999) 303–320.
[45] M.E. Fabiyi, R.L. Skelton, The application of oscillatory flow mixing to photocatalytic wet oxidation, J. Photochem. Photobiol. A: Chem. 129 (1999) 17–24.
[46] I. Ilisz, Z. László, A. Dombi, Investigation of the photodecomposition of phenol in near-UV-irradiated aqueous TiO_2 suspensions. I: Effect of charge-trapping species on the degradation kinetics, Appl. Catal. A: Gen. 180 (1999) 25–33.
[47] G. Li Puma, P.L. Yue, Enhanced photocatalysis in a pilot laminar falling film slurry reactor, Ind. Eng. Chem. Res. 38 (1999) 3246–3254.
[48] J. Bangun, A.A. Adesina, The photodegradation kinetics of aqueous sodium oxalate solution using TiO_2 catalyst, Appl. Catal. A: Gen. 175 (1998) 221–235.
[49] M.S.T. Gonqalves, A.M.F. Oliveira-Campos, E.M.M.S. Pinto, P.M.S. Plasência, M.J.R.P. Queiroz, Photochemical treatment of solutions of azo dyes containing TiO_2, Chemosphere 39 (5) (1999) 781–786.
[50] R.I. Bickley, M.J. Slater, W.-J. Wang, Engineering development of a photocatalytic reactor for waste water treatment, Process Safety Environ. Protect. 83 (2005) 205–216.
[51] R.J. Brandi, O.M. Alfano, A.E. Cassano, Rigorous model and experimental verification of the radiation field in a flat-plate solar collector simulator employed for photocatalytic reaction, Chem. Eng. Sci. 54 (1999) 2817–2827.
[52] D.F. Ollis, Solar-assisted photocatalysis for water purification: issues, data, questions, in: E. Pellizetti, M. Schiavello (Eds.), Photochemical Conversion and Storage of Solar Energy, Kluwer Academic Publishers, Netherlands, 1991, pp. 593–622.
[53] C.S. Zalazar, R.L. Romero, C.A. Martín, A.E. Cassano, Photocatalytic intrinsic reaction kinetics I: mineralization of dichloroacetic acid, Chem. Eng. Sci. 60 (2005) 5240–5254.
[54] C.S. Zalazar, Doctoral Thesis, Universidad Nacional del Litoral, 2003.
[55] C.S. Zalazar, M.D. Labas, C.A. Martín, R.J. Brandi, O.M. Alfano, A.E. Cassano, The extended use of actinometry in the interpretation of photochemical reaction engineering data, Chem. Eng. J. 109 (2005) 67–81.
[56] P.A. Davidson, Turbulence. An Introduction for Scientists and Engineers, Oxford University Press, 2004.
[57] R. Taylor, R. Krishna, Multicomponent Mass Transfer, Wiley, New York, 1993.
[58] W.M. Kays, M.E. Crawford, Convective Heat and Mass Transfer, MacGraw-Hill, New York, 1980.
[59] R.B. Bird, W.E. Stewart, W.N. Lightfoot, Transport Phenomena, New York, Wiley, 1960.
[60] G.F. Froment, K.B. Bischoff, Chemical Reactor Analysis and Design, Wiley, New York, 1990.
[61] W.M. Deen, Analysis of Transport Phenomena, Oxford University Press, 1998.
[62] R.E. Treybal, Mass Transfer Operation, MacGraw-Hill, New York, 1981.
[63] M.N. Özisik, Radiative Transfer and Interactions with Conduction and Convection, Wiley, New York, 1973.
[64] A.E. Cassano, C.A. Martín, R.J. Brandi, O.M. Alfano, Photoreactor analysis and design: fundamentals and applications, Ind. Eng. Chem. Res. 34 (1995) 2155–2201.
[65] O.M. Alfano, M.I. Cabrera, A.E. Cassano, Modeling of light scattering in photochemical reactors, Chem. Eng. Sci. 49 (1994) 5327–5346.
[66] M.L. Satuf, R.J. Brandi, A.E. Cassano, O.M. Alfano, Experimental method to evaluate the optical properties of aqueous titanium dioxide suspensions, Ind. Eng. Chem. Res. 44 (2005) 6643–6649.
[67] R. Siegel, J.R. Howell, Thermal Radiation Heat Transfer, fourth ed., Hemisphere Publishing Corp, Bristol, PA, 2002.
[68] H.C. Van de Hulst, Multiple Light Scattering, Academic Press, New York, 1980.
[69] M.D. Labas, C.S. Zalazar, R.J. Brandi, C.A. Martín, A.E. Cassano, Scaling Up of a photoreactor for formic acid degradation employing hydrogen peroxide and UV radiation, Helv. Ch. Acta 85 (2002) 82–95.
[70] A.K. Agrawal, R.S. Peckover, Nonuniform grid generation for boundary layer problems, Comput. Phys. Commun. 19 (1980) 171–178.
[71] R.C. Reid, J.M. Prausnitz, B.E. Poling, The Properties of Gases and Liquid, fourth ed., Mc Graw-Hill Book Company, 1987.
[72] R.C. Reid, J.M. Prausnitz, T.K. Sherwood, The Properties of Gases and Liquid, third ed., Mc Graw-Hill Book Company, 1977.
[73] J.H. Perry, Chemical Engineers' Handbook, McGraw-Hill, New York, 1997.
[74] J. Duderstadt, W. Martin, Transport Theory, Wiley, New York, 1979.
[75] C.S. Turchi, D.F. Ollis, Photocatalytic degradation of organic water contaminants: mechanisms involving hydroxyl radical attack, J. Catal. 122 (1) (1990) 178–192.
[76] O.M. Alfano, M.I. Cabrera, A.E. Cassano, Photocatalytic reactions involving hydroxyl radical attack. I. Reaction kinetics formulation with explicit photon absorption effects, J. Catal. 172 (1997) 370–379.